Desalination and Water Treatment
www.deswater.com

doi: 10.5004/dwt.2023.29506

292 (2023) 122–130
April

Facile synthesis of Cu-complex for visible light photodegradation of organic dyes and sulfonamide antibiotics with added H_2O_2

Dawei Wang[a,*], Xuebing Ji[b], Zhengjun Shi[a]

[a]*Key Laboratory for Forest Resources Conservation and Utilization in the Southwest Mountains of China, Ministry of Education, Southwest Forestry University, Kunming 650224, P.R. China, Tel.: +86 15812026167/+86 15908899596; emails: wdwchem@163.com (D.W. Wang), shizhengjun1979@163.com (Z.J. Shi)*
[b]*Key Laboratory of State Forestry and Grassland Administration on Highly-Efficient Utilization of Forestry Biomass Resources in Southwest China, Southwest Forestry University, Kunming 650224, P.R. China, Tel.: +86 15902679882; email: JXBLJR2021@163.com*

Received 15 October 2022; Accepted 22 March 2023

ABSTRACT

In this article, copper complex $[Cu(biba)_2]\cdot H_2O$ (biba = 2-(1H-benzoimidazol-2-yl)benzoic acid) was synthesized via hydrothermal method, and structurally characterized by single-crystal X-ray diffraction, powder X-ray diffraction, UV-Vis diffuse reflectance spectra, Raman spectra and Fourier-transform infrared spectroscopy. $[Cu(biba)_2]\cdot H_2O$ exhibited good photocatalytic activities in degradation of methylene blue (MB) dye and sulfadiazine (SD) antibiotic under visible light with added H_2O_2. The degradation efficiency of MB was up to 93.1% after reacting for 80 min, and the degradation efficiency of SD was over 96.8% after reacting for 60 min. The degradation kinetics of MB and SD under $[Cu(biba)_2]\cdot H_2O/H_2O_2$ catalytic system was studied, and the observed first-order kinetics rate constants (k) were 0.0340 and 0.0573 min^{-1}, respectively. Based on the experimental results, a reasonable mechanism was proposed to interpret the photo-Fenton oxidation process.

Keywords: Photocatalysis, Organic dye, Sulfadiazine antibiotic, Copper complex

1. Introduction

Presently, various organic pollutants in wastewater, such as industrial dyes and antibiotics, discharged from textile industry, medical industry and livestock industry have received great concerns because they are difficult to degrade and harmful to human's health [1]. The efficient removal of these pollutants from wastewaters is very important from the perspective of environmental protection. Especially, the presence of antibiotics in the water environment has become an issue of international concern, because some pharmaceutical agents are associated with adverse effects to aquatic life, even at very low concentrations [2]. In order to protect the environment, many attempts are being made to minimize or fully remove the synthetic dyes and antibiotics from aquatic systems [3,4]. However, the most commonly used biodegradation method is time-consuming and incomplete. Recently, photocatalysis is considered as an efficient and clean technology for contaminants abatement in aqueous media, which is a good option for removing of industrial dyes and antibiotics from wastewaters [5]. In view of visible light covering the main band of solar light, the photocatalysts driven by visible light have attracted considerable attention.

In the past decade, many researches have dedicated to the preparation of various heterogeneous copper-based catalysts and their application in photocatalytic degradation of organic pollutants [6]. For instance, copper oxides (CuO and Cu_2O) are available to absorb visible light and exhibit good photocatalytic activity in degraded organic dyes with added H_2O_2 [7]. As a class of narrow band gap semiconductor materials Cu-complexes also attracted tremendous

* Corresponding author.

interest for their unique optical and charge transport properties [8]. Cu-complexes are found to be efficient catalysts for degradation of industrial dyes in the presence of H_2O_2, which can be seen as a class of photo-Fenton catalysts [9,10]. Studies have shown that, with added H_2O_2, copper catalysts have shown the ability to produce •OH in a Fenton-like system [11]. Therefore, the catalytic activity of copper catalysts is greatly enhanced when H_2O_2 is present as the oxidant [6]. Moreover, in photo-Fenton reaction, H_2O_2 is considered as an electron acceptor to promote the electron–hole separation and decompose to form a certain amount of •OH by accepting electrons [7]. Earlier, we synthesized a one-dimensional Cu-complex $[Cu(tba)_2(H_2O)]\cdot 2H_2O$, which exhibited good photocatalytic activity towards organic dyes and phytohormones under UV irradiation in the presence of H_2O_2 [12]. In spite of extensive researches in the past few decades, the investigation of highly efficient visible light induced heterogeneous photo-Fenton catalysts is of important and immense challenge. Considering the structural diversity of Cu-complexes, our work will focus on the design and synthesis of new copper complexes and investigates their applications in photodegradation of organic pollutants.

In this work, a new Cu-complex $[Cu(biba)_2]\cdot H_2O$ has been hydrothermally synthesized and structurally characterized by single-crystal X-ray diffraction. Photocatalytic degradation of methylene blue dye and sulfadiazine antibiotic by $[Cu(biba)_2]\cdot H_2O$ were performed under visible light irradiation in the presence of H_2O_2. Finally, a photo-Fenton oxidation mechanism was proposed based on the good photocatalytic performance of $[Cu(biba)_2]\cdot H_2O/H_2O_2$ system. As a new copper complex, the as-prepared $[Cu(biba)_2]\cdot H_2O$ has the advantages of low cost, high catalytic activity, and high mechanical stability, which is a promising photocatalyst in sewage purification.

2. Experimental set-up

2.1. Materials

All reagents employed in the experiments were commercially available, and all solutions were prepared with doubly distilled water. The reagents 1,2-phenylenediamine, 2-formylbenzoic acid and $Cu(NO_3)_2\cdot 3H_2O$ were purchased from Adamas Co., Ltd., (Shanghai, China). Methylene blue, sulfadiazine and hydrogen peroxide (H_2O_2, 30%) were purchased from Sinopharm Chemical Reagent Co., Ltd., China.

2.2. Characterization

The single-crystal X-ray diffraction data of Cu-complex was collected on a Bruker AXS smart APEX II CCD diffractometer equipped with graphite monochromated Mo-Kα radiation (λ = 0.71073 Å). The crystal structure was solved with the direct method and refined by full-matrix least squares on F^2 using SHELXTL-2014 program [13]. The non-hydrogen atoms were refined anisotropically, and all hydrogen atoms were added theoretically. The elemental analysis was carried out with a Vario-EL III element analyzer. The powder X-ray diffraction (XRD) data was characterized by a Rigaku TTR(III) X-ray diffractometer with Cu-Kα radiation (λ = 1.5406 Å). Fourier-transform infrared spectra (FTIR) were recorded from KBr pellet in a Varian 640-IR spectrophotometer with a range of 400–4,000 cm^{-1}. Raman spectrum was measured on a Renishaw inVia Raman microscope in the range of 3,200–100 cm^{-1}. UV-Vis diffuse reflectance spectrum was recorded using a Lambda 950 spectrophotometer with $BaSO_4$ as reference standard. Electron spin resonance (ESR) measurement was performed on a Bruker EMXplus ESR spectrometer. Nuclear magnetic resonance (^{1}H NMR) was recorded in a Bruker AVANCEIII, 400 MHz spectroscopy. Thermal analysis was performed on a Mettler Toledo TGA/DSC 1/1600 (Switzerland) thermal analyzer from room temperature to 900°C under N_2 atmosphere at a heating rate of 10°C min^{-1}. The absorbance of methylene blue and sulfadiazine solution during photocatalysis were detected using a Persee TU-1901 spectrophotometer (Beijing, China).

2.3. Syntheses of 2-(1H-benzoimidazol-2-yl)benzoic acid (biba)

Ligand 2-(1H-benzoimidazol-2-yl)benzoic acid (biba) was prepared via condensation of 1,2-phenylenediamine and 2-formylbenzoic acid according to the improved procedure from the literature [14]. A solution of 2-formylbenzoic (3.04 g, 20 mmol) in 10 mL absolute ethanol was added slowly to the solution of 1,2-phenylenediamine (2.16 g, 20 mmol) in absolute ethanol (20 mL), and the resulting mixture was stirred at 60°C for 3 h, giving a light-yellow precipitate. After vacuum filtration, washing with 3 mL of ethanol, vacuum drying, 4.28 g light yellow solid powder was obtained, yield 90%. Anal. (%) calc. for $C_{14}H_{10}N_2O_2$: C, 70.58; H, 4.23; N, 11.76. Found: C, 70.56; H, 4.25; N, 11.80. Infrared (IR) (KBr pellet, cm^{-1}): 3467 (br, O–H), 3,066 (m), 1,604 (s), 1,453 (s), 1,373 (s), 856 (m), 734 (m), 686 (m), 615 (m). ^{1}H-NMR (400 MHz, d-DMSO): δ (ppm) 7.88 (d, 2H, –Ph), 7.82–7.78 (m, 4H, –Ph), 7.71–7.67 (m, 2H, –Ph), 7.12 (br N–H). The IR and ^{1}H-NMR spectra of biba are shown in Figs. S1 and S2, respectively, and the molecular structure of biba can be seen from Fig. 1b.

2.4. Preparation of Cu-complex $[Cu(biba)_2]\cdot H_2O$

To a 15 mL pressure-resistant glass reactor with a Teflon plastic cover, 24 mg $Cu(NO_3)_2\cdot 3H_2O$ (0.1 mmol), 24 mg 2-(1H-benzoimidazol-2-yl)benzoic acid (Hbiba, 0.1 mmol) and 6 mL mixed solvent ($V_{ethanol}$: V_{water} = 1:1) were added. The mixture was stirred at room temperature for 15 min, then sealed and heated at 100°C for 48 h in an oven. After cooling to room temperature, red-brown block crystals were obtained with a yield 68% (Fig. 1a). Elemental Anal. Calc. for $C_{28}H_{22}CuN_4O_6$(%): C 58.58, H 3.86, N 9.76; found: C 58.62, H 3.81, N 9.80. IR (KBr, cm^{-1}): 3,445(m), 3,275(m), 3,065(w), 1,562(s), 1,427(s), 1,285(w), 993(m), 752(s), 581(w) (Fig. 2b). The crystallographic and refinement data of the synthesized Cu-complex $[Cu(biba)_2]\cdot H_2O$ are listed in Table 1.

2.5. Photocatalytic experiments

The photocatalytic behavior of $[Cu(biba)_2]\cdot H_2O$ was tested for the degradation of methylene blue (MB) dye and sulfadiazine (SD) antibiotic under visible light irradiation at room temperature. The procedure was as follows: 50 mg $[Cu(biba)_2]\cdot H_2O$ as heterogeneous catalyst was mixed together with 50 mL of MB (10 mg/L), followed by

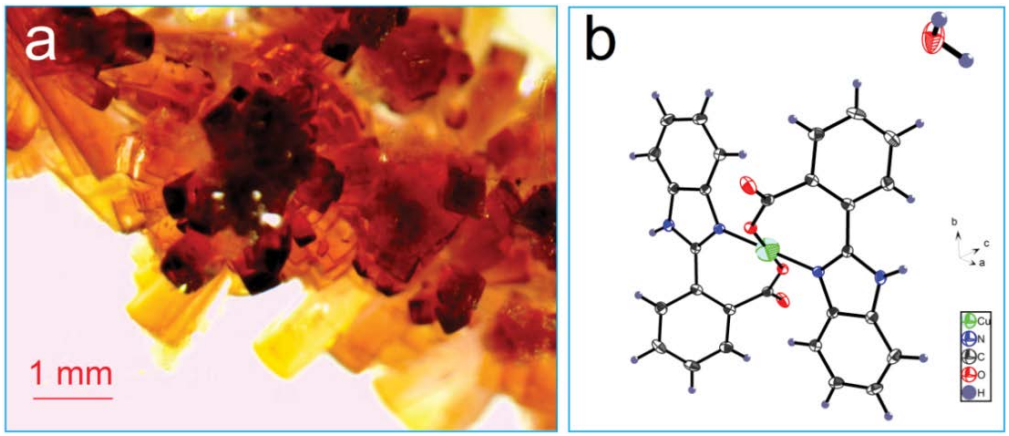

Fig. 1. Single-crystal photomicrograph (a) and molecular structure (b) of $[Cu(biba)_2]\cdot H_2O$.

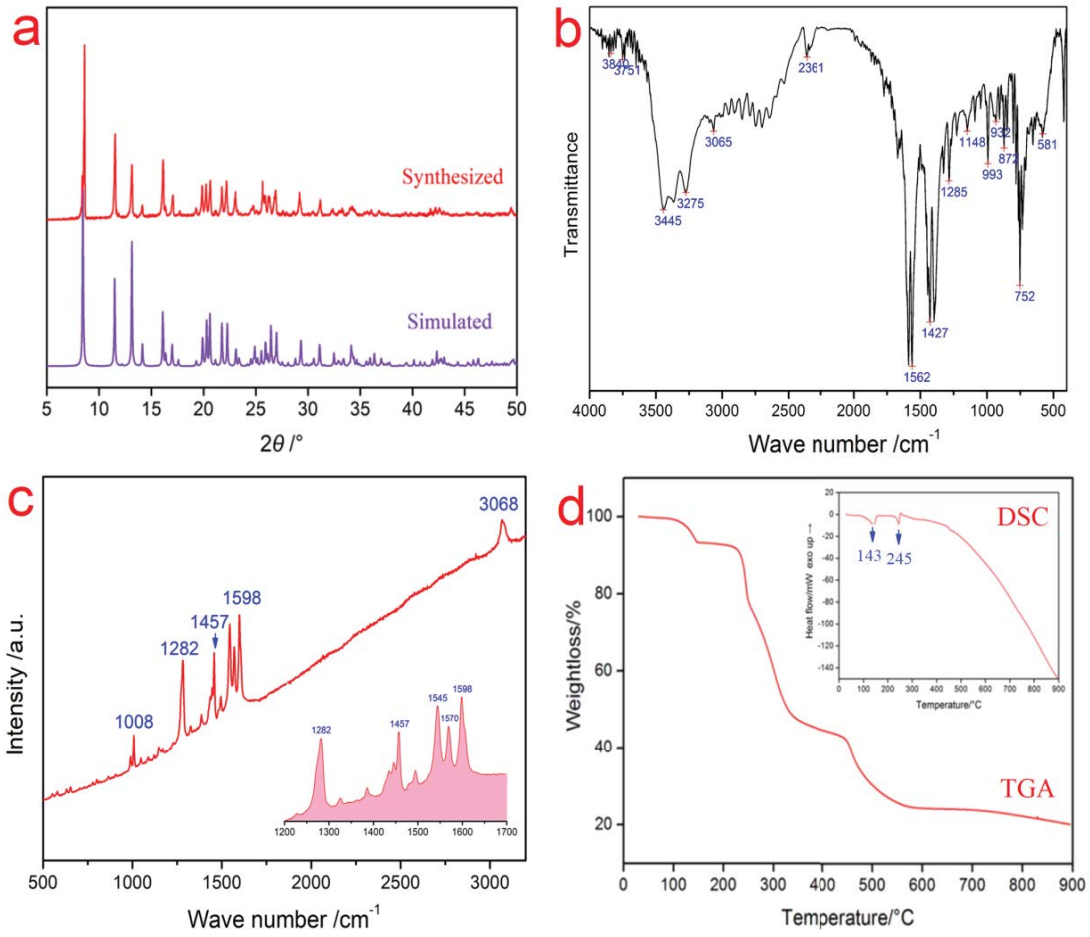

Fig. 2. (a) XRD patterns of $[Cu(biba)_2]\cdot H_2O$, (b) FTIR spectrum of $[Cu(biba)_2]\cdot H_2O$, (c) Raman spectrum of $[Cu(biba)_2]\cdot H_2O$ and (d) TGA and DSC curves of $[Cu(biba)_2]\cdot H_2O$.

magnetically stirring in the dark for 1 h to ensure the adsorption equilibrium. Then, 0.1 mL H_2O_2 (30%) was added, and the mixed solution was exposed to a power of 100 mW/cm^2 visible light irradiation from a 300 W Xe lamp (CEL-HXF300-T3, CEAULIGHT Co., Ltd., Beijing) with a 420 nm cut-off filter. The solution was kept stirring during irradiation. At different time intervals, about 2.5 mL analytical samples were withdrawn and analyzed by a UV–vis spectrophotometer. Control experiments were performed under the similar conditions but without catalyst or without H_2O_2.

Table 1
Crystallographic and refinement data for complex $[Cu(biba)_2]\cdot H_2O$

Complex	$[Cu(biba)_2]\cdot H_2O$
Empirical formula	$C_{28}H_{22}CuN_4O_6$
Formula weight	574.04
Temperature (K)	296(2)
Wavelength (nm)	0.71073
Crystal system	Monoclinic
Space group	$P2_1/n$
Crystal size (mm)	0.26 × 0.19 × 0.16
a (Å)	11.566(7)
b (Å)	7.6022(5)
c (Å)	15.2589(9)
α (°)	90
β (°)	107.98(10)
γ (°)	90
Volume (Å^3)	1,276.10(14)
Z	2
ρ_{calc}, g/cm^3	1.494
F(000)	590
Unique data	2,246
R(int)	0.0235
Restraints/parameters	0/222
Final R indices [I > 2sigma(I)]	R_1 = 0.0261, wR_2 = 0.0779
Goodness-of-fit on F^2 (S)	1.151
L. diff. peak/hole (e Å^{-3})	0.314/–0.255

Degradation efficiencies (DE) of MB dye were calculated by the following formula [8,15]:

$$\mathrm{DE} = \frac{\left(A_0 - A_t\right)}{A_0} \times 100\% \quad (1)$$

where A_t was the absorbance of MB solution at different time intervals, and A_0 was the initial absorbance of MB solution (t = 0). The photocatalytic degradation experiments of sulfadiazine (SD) were carried out using the method similar to that of MB.

3. Results and discussion

3.1. Crystal structure of $[Cu(biba)_2]\cdot H_2O$

Single-crystal X-ray diffraction analysis reveals that the synthesized Cu-complex $[Cu(biba)_2]\cdot H_2O$ crystallizes in the monoclinic space group $P2_1/n$. As shown in Fig. 1b, the central Cu atom is four-coordinated by two oxygen atoms come from carboxyl group with Cu–O distance of 1.9255(13) Å, and two nitrogen atoms from imidazole group with Cu–N distance of 1.9518(15) Å, forming a planar quadrangle configuration. The selected bond lengths and angles for $[Cu(biba)_2]\cdot H_2O$ are listed in Table 2. In addition, the asymmetric unit of Cu-complex consists of one lattice water molecule.

Table 2
Selected bond lengths (Å) and angles (°) for $[Cu(biba)_2]\cdot H_2O$

Cu1-O2	1.9255(13)	O2^1-Cu1-N1^1	89.98(6)
Cu1-O2^1	1.9255(13)	O2-Cu1-N1^1	90.02(6)
Cu1-N1	1.9518(15)	O2^1-Cu1-N1	90.02(6)
Cu1-N1^1	1.9518(15)	O2-Cu1-N1	89.98(6)
N1-C6	1.337(2)	O2^1-Cu1-O2	180.00(8)
N1-C3	1.402(2)	N1^1-Cu1-N1	180.00(9)

Symmetry transformations used to generate equivalent atoms: ^{1}–x + 2, –y + 1, –z.

3.2. Characterization of $[Cu(biba)_2]\cdot H_2O$

The crystalline structure of $[Cu(biba)_2]\cdot H_2O$ was further examined by X-ray powder diffraction (XRD) in a 2θ range of 5°–50°. As shown in Fig. 2a, the experimental XRD pattern agree well with the simulated pattern generated on the basis of the single-crystal data of $[Cu(biba)_2]\cdot H_2O$, suggesting the phase purity of the synthesized product.

In the FTIR spectrum of $[Cu(biba)_2]\cdot H_2O$, no strong peak is found in the region 1,690–1,730 cm^{-1} indicates deprotonation of the carboxylic groups [16]. The asymmetric and symmetric stretching vibrations of carboxylate group are observed at about 1,562 and 1,427 cm^{-1}, respectively [17]. The two broad bands appeared at 3,445 and 3,275 cm^{-1} can be assigned to O–H stretching vibration of the lattice water and N–H stretching vibration of the imidazole ring, respectively [18]. The weak peak at 3,065 cm^{-1} is attributed to sp^2 C–H stretching vibrations of benzene rings. Moreover, the weak peak at 581 cm^{-1} can be assigned to the vibration of Cu–O coordination bond [19].

The Raman spectrum of $[Cu(biba)_2]\cdot H_2O$ is presented in Fig. 2c, in which the strong peaks at 1,598 and 1,570 cm^{-1} can be assigned to the symmetric vibrations of C=C and C=N groups from the ligand [20]. The strong peaks at 1,545 and 1,457 cm^{-1} can be assigned to the asymmetric and symmetric vibrations of carboxylate group, respectively. Moreover, the peak at 1,008 cm^{-1} is attributed to the skeleton vibrations of benzene ring, and the broad peak at about 3,068 cm^{-1} is related to –C–H stretching vibrations of benzene ring [21].

To evaluate the thermal properties of complex $[Cu(biba)_2]\cdot H_2O$, thermal gravimetric analysis (TGA) and differential scanning calorimetry analysis (DSC) were performed under N_2 atmosphere. As shown in Fig. 2d, the thermal decomposition of $[Cu(biba)_2]\cdot H_2O$ occurs in a multi-step process. The first step takes place in the range of 81°C–175°C with a weight loss of 6.5% (calcd. 6.3%), corresponding to the loss of a lattice water. A rapid breakdown of the molecular skeleton was found after 220°C. Until heated to 570°C, the residue is Cu_2O with a residual weight of 24.8% (calcd. 25.1%). It can be seen from the DSC curve that the sample is endothermic throughout the decomposition process. However, two sharp endothermic peaks are found at 143°C and 245°C. The endothermic peak at 143°C can be assigned to the loss of lattice water, while the peak at 245°C corresponds to the rapid weight loss process in which the skeleton of the Cu-complex begins to decompose. Thermal analyses indicated that the synthesized $[Cu(biba)_2]\cdot H_2O$ has good thermal stability.

3.3. Optical properties of $[Cu(biba)_2]\cdot H_2O$

The UV-Vis diffuse reflectance spectrum was employed to characterize the optical absorbance of complex $[Cu(biba)_2]\cdot H_2O$. As shown in Fig. 3a, complex $[Cu(biba)_2]\cdot H_2O$ shows the light absorption in both the visible and ultraviolet region. The strong absorption bands at ultraviolet region can be attributed to the π→π* and n→π* electronic transitions of the biba ligand [22]. The broad absorption band at 510 nm in the visible light region is ascribed to the ligand-to-metal charge transfer (LMCT) [23]. Based on the optical absorption spectra, the band gap energy (E_g) of $[Cu(biba)_2]\cdot H_2O$ is calculated by the equation [24]:

$$\alpha h\nu = A\left(h\nu - E_g\right)^{n/2} \tag{2}$$

where α, h, ν, and A is absorption coefficient, Planck constant, the light frequency, and proportionality constant, respectively. Apparently, the as-synthesized Cu-complex exhibits strong visible light adsorption ability and possesses a narrow band gap of 1.91 eV.

3.4. Photocatalytic activity

The photocatalytic activity of $[Cu(biba)_2]\cdot H_2O$ was assessed by measuring the decomposition of methylene blue (MB) and sulfadiazine (SD) solution under visible light irradiation in the presence of hydrogen peroxide. It should be noted that, after stirring in the dark for 1 h to reach the adsorption equilibrium, the absorbance (Abs) of MB and SD solution were reduced by 6.8% and 7.5%, respectively, indicating a moderate adsorption capacity of $[Cu(biba)_2]\cdot H_2O$. As shown in Fig. 4a, under the catalysis of $[Cu(biba)_2]\cdot H_2O/H_2O_2$, the absorption intensities of MB decrease gradually along with prolonging of radiation time. The degradation efficiency of MB was calculated based on the absorption at 664 nm. As shown in Fig. 4b, the degradation efficiencies of MB are about 27.9% and 83.5% after reacting for 20 and 60 min, respectively. Notably, the degradation efficiency of MB is up to 93.1% after reacting for 80 min under the catalysis of $[Cu(biba)_2]\cdot H_2O$, indicating that the MB dye is nearly completely decomposed. In addition, comparative experiments were performed only with H_2O_2. As depicted in Fig. 4b, after reacting for 80 min the degradation of MB hardly proceed in absence of catalyst, with a degradation efficiency of 11.8%.

Sulfadiazine (SD) was selected as a model of sulfonamide antibiotic to test the photocatalytic activity of $[Cu(biba)_2]\cdot H_2O$ under visible light irradiation. SD has a characteristic absorption peak at 264 nm in UV region, and the degradation efficiencies of SD are calculated based on the absorption at 264 nm via a spectrometer. As shown in Fig. 4c, the absorption intensities of SD solution decrease gradually with prolonging of irradiation time, which indicates a rapid degradation of SD. The degradation efficiency of SD reached 96.8% after irradiating for 60 min, indicating almost completely degraded of SD. It can be found from the comparative experiment that the degradation efficiency of SD is only 11.2% without the Cu-complex catalyst, although in the presence of the H_2O_2 oxidant (Fig. 4d). Moreover, without catalyst and H_2O_2, there was no apparent degradation for MB and SD when the solution was treated with visible light, which was also found by other report [6].

The photocatalytic degradation kinetics of MB and SD solution were analyzed by the pseudo-first-order model according to the following equation [25,26]:

$$\ln\left(\frac{C_0}{C_t}\right) = k \times t \tag{3}$$

where C_0 is the initial concentration of substrate, C is the concentration at reaction time t (min), and k (min^{-1}) is the reaction rate constant of first-order kinetic model. As shown in Fig. 5, the $\ln(C_0/C_t)$ plot shows a linear relationship with the reaction time t, which means that the photocatalytic degradation process of MB and SD fit well with the pseudo-first-order correlation. The reaction rate constants (k) are given by the slopes of linear fit and estimated to be 0.0340 and 0.0573 min^{-1} for MB and SD, respectively. By comparing the two rate constants (k), it is found that the degradation rate of SD is higher than that of MB under the same catalytic conditions.

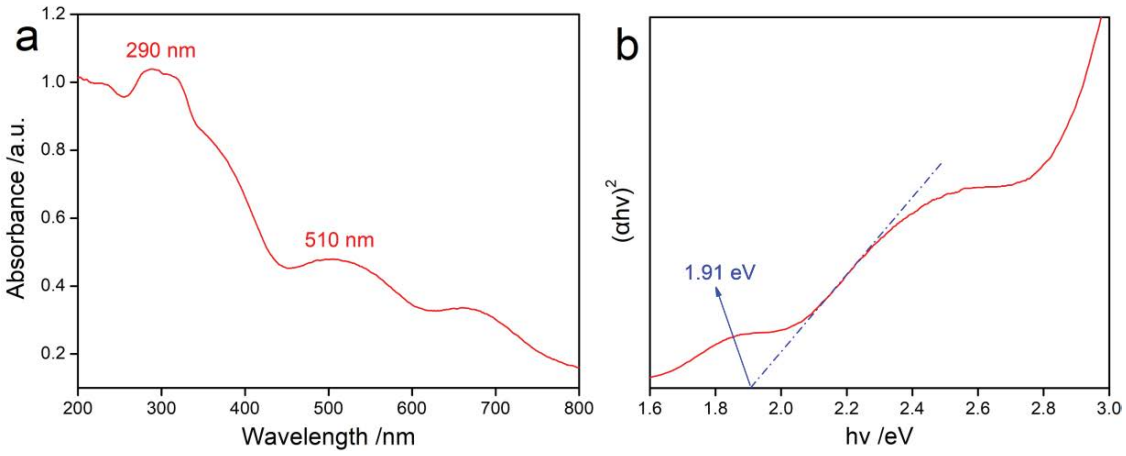

Fig. 3. UV-Vis diffuse reflectance spectrum (a) and the calculated band gap energy (b) of $[Cu(biba)_2]\cdot H_2O$.

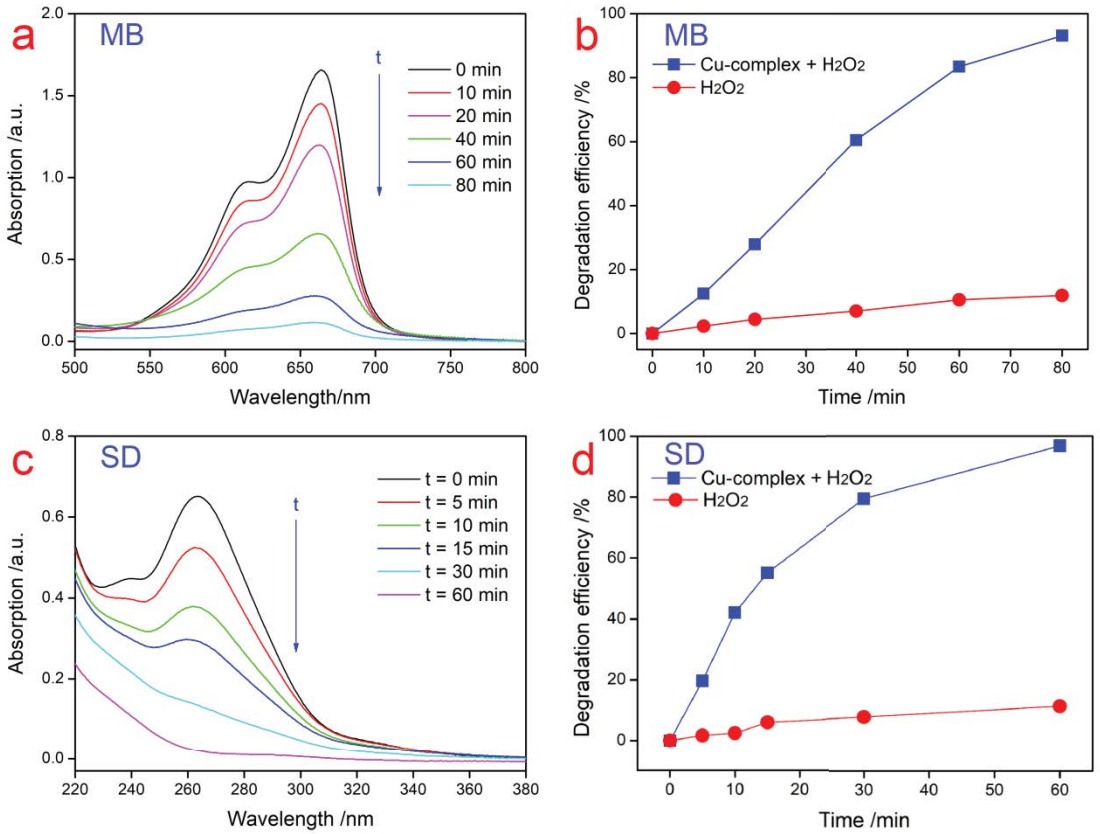

Fig. 4. Absorption curves (a) and degradation efficiencies (b) of methylene blue at different time intervals under the catalysis of $[Cu(biba)_2]\cdot H_2O$; the absorption curves (c) and degradation efficiencies (d) of sulfadiazine at different time intervals under the catalysis of $[Cu(biba)_2]\cdot H_2O$.

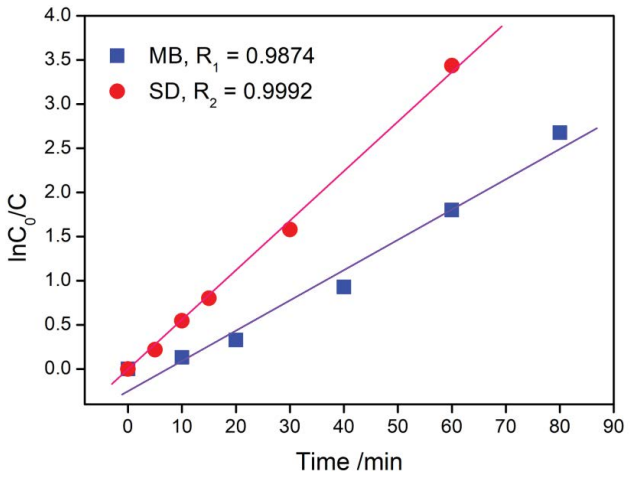

Fig. 5. First-order kinetic plot of $\ln(C_0/C)$ vs. reaction time (MB: $y = 0.0340x - 0.2149$, SD: $y = 0.0573x - 0.04928$).

3.5. Photocatalytic mechanism

Trapping experiments were carried out by adding 0.2 mL t-butyl alcohol (TBA) and 10 mg benzoquinone (BQ) to MB solution as •OH and $•O_2^-$ scavengers, respectively [27]. As shown in Fig. 6a, the introducing of BQ has no significant effect on the degradation efficiency of MB. However, the degradation efficiency of MB is significantly inhibited by adding TBA to trap •OH, indicating that the •OH is the key active species in photocatalytic process. In order to further demonstrate the generation of •OH radical in the degradation process, ESR measurement by using DMPO as spin-trapping agent was carried out in $[Cu(biba)_2]\cdot H_2O/H_2O_2$ system under visible light irradiation for 10 min. The results show 4-fold characteristic peaks with intensity ratio of 1:2:2:1 (Fig. 6a), which further confirms the generation of •OH radical in the photocatalytic process [1].

The photocatalytic mechanism of Cu-compounds and Cu-complexes in catalyzing the degradation of various organic pollutants has been reported by many researchers [28]. Based on the photocatalytic experiments and the trapping experiments above, the possible photodegradation mechanism of MB and SD in the presence of $[Cu(biba)_2]\cdot H_2O/H_2O_2$ is illustrated in Fig. 6b. When exposed to visible light irradiation, photons were absorbed by $[Cu(biba)_2]\cdot H_2O$, and the electrons were excited from the highest occupied molecular orbital (HOMO) of $[Cu(biba)_2]\cdot H_2O$ to the lowest unoccupied molecular orbital (LUMO), as illustrated in Eq. (4). Thus, the HOMO energy level (h^+) captured electrons from aqueous solution to return to its stable state and generated hydroxyl radicals (•OH) (Eq. 5). As expected, there was a synergetic effect resulting from the combination of Cu-complex with H_2O_2. The addition of H_2O_2 to the reaction system significantly promoted the photocatalytic reaction,

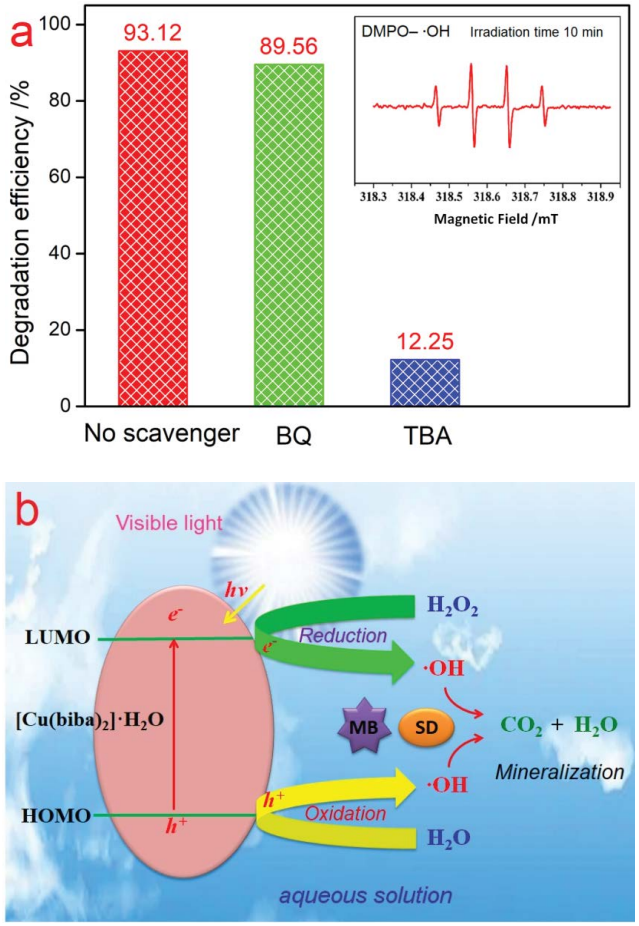

Fig. 6. (a) Effect of scavengers on the degradation efficiencies of methylene blue dye under visible light irradiation (methylene blue concentration 10 mg/L, catalyst 50 mg, irradiation time 80 min) and the ESR spectra of DMPO spin-trapping adducts in $[Cu(biba)_2]\cdot H_2O/H_2O_2$ system (inserted image) and (b) the proposed photodegradation mechanism of methylene blue and sulfadiazine in the presence of $[Cu(biba)_2]\cdot H_2O/H_2O_2$ under visible light.

because Cu-complex could catalyze the decomposition of H_2O_2 to produce more $^{\bullet}OH$ radicals [Eq. (6)] [11]. In this process the H_2O_2 acted as an acceptor of photogenerated electrons. Besides, the slow spontaneous decomposition of hydrogen peroxide under visible light also produced small amounts of $^{\bullet}OH$ [Eq. (7)]. Finally, the $^{\bullet}OH$ radicals acted as strong oxidant to mineralize the organic dyes and sulfonamide antibiotics into CO_2 and H_2O. Some crucial steps that correspond to the photocatalytic process are shown in the following equations:

$$Cu(II)-complex+hv \rightarrow Cu(I)-complex+e^{-}+h^{+} \quad (4)$$

$$H_2O+h^{+} \rightarrow {}^{\bullet}OH+H^{+} \quad (5)$$

$$Cu(I)-complex+H_2O_2+e^{-} \rightarrow Cu(II)-complex+OH^{-}+{}^{\bullet}OH \quad (6)$$

$$H_2O_2+hv \rightarrow 2{}^{\bullet}OH \quad (7)$$

4. Conclusions

In summary, crystals of Cu-complex $[Cu(biba)_2]\cdot H_2O$ was successfully synthesized via hydrothermal method and well characterized, which exhibited excellent thermal stability and visible light absorption properties. The synthesized Cu-complex exhibited good photocatalytic activity in the degradation of water pollutants MB and SD under visible light. It was found that the addition of H_2O_2 to the reaction system significantly promoted the photodegradation of MB and SD. Finally, the photocatalytic mechanism was proposed according to the photocatalytic experiments and radical trapping experiments. This study provides a simple method for using solar energy to degrade organic pollutants in wastewater.

Conflict of interest

The authors declare that they have no conflict of interest.

Acknowledgements

This work was financially supported by the National Natural Science Foundation of China (No. 32260427), Yunnan Fundamental Research Projects (No. 202001AT070141), Yunnan Agricultural Basic Research Special Projects (No. 202101BD070001-086), and the open fund of Key Laboratory for Forest Resources Conservation and Utilization in the Southwest Mountains of China, Ministry of Education (No. KLESWFU–201909).

References

[1] X.K. Tang, Z.S. Li, K. Liu, X. Luo, D. He, M. Ao, Q. Peng, Sulfidation modified Fe_3O_4 nanoparticles as an efficient Fenton-like catalyst for azo dyes degradation at wide pH range, Powder Technol., 376 (2020) 42–51.
[2] M.F.N. Secondes, V. Naddeo, V. Belgiorno, F. Ballesteros, Removal of emerging contaminants by simultaneous application of membrane ultrafiltration, activated carbon adsorption, and ultrasound irradiation, J. Hazard. Mater., 264 (2014) 342–349.
[3] Y.L. Zhang, R. Ding, S.N. Li, Y.C. Jiang, M.C. Hu, Q.G. Zhai, Ionothermal design of crystalline halogeno(cyano)cuprate family: structure diversity, solid-state luminescence, and photocatalytic performance, Inorg. Chem., 56 (2017) 7161–7174.
[4] S. Jafari, B. Yahyaei, E. Kusiak-Nejman, M. Sillanpaa, The influence of carbonization temperature on the modification of TiO_2 in the removal of methyl orange from aqueous solution by adsorption, Desal. Water Treat., 57 (2016) 18825–18835.
[5] D.W. Wang, J. Yang, H.Y. Yang, P. Zhao, Z.J. Shi, Fe-complex modified cellulose acetate composite membrane with excellent photo-Fenton catalytic activity, Carbohydr. Polym., 296 (2022) 119960, doi: 10.1016/j.carbpol.2022.119960.
[6] P. Liu, C. Li, X. Kong, G. Lu, J. Xu, F. Ji, X. Liang, Photocatalytic degradation of EDTA with UV/Cu(II)/H_2O_2 process, Desal. Water Treat., 51 (2013) 7555–7561.
[7] X. Deng, C. Wang, M. Shao, X. Xu, J. Huang, Low-temperature solution synthesis of CuO/Cu_2O nanostructures for enhanced photocatalytic activity with added H_2O_2: synergistic effect and mechanism insight, RSC Adv., 7 (2017) 4329–4338.
[8] S.E.H. Etaiw, M.M. El-bendary, Crystal structure, characterization and catalytic activities of Cu(II) coordination

complexes with 8-hydroxyquinoline and pyrazine-2-carboxylic acid, Appl. Organomet. Chem., 32 (2018) e4213, doi: 10.1002/aoc.4213.
[9] Y.P. Zhang, H.T. Cui, B.Y. Zhang, A. Tian, Three Keggin-based complexes modified by an asymmetric ligand: structures, electrochemical, photocatalytic and fluorescence sensing properties, Transition Met. Chem., 47 (2022) 229–238.
[10] A.S. Elsherbiny, H.A. El-Ghamry, Synthesis, characterization, and catalytic activity of new Cu(II) Complexes of Schiff Base: effective catalysts for decolorization of acid red 37 dye solution, Int. J. Chem. Kinet., 47 (2015) 162–173.
[11] J.K. Kim, I.S. Metcalfe, Investigation of the generation of hydroxyl radicals and their oxidative role in the presence of heterogeneous copper catalysts, Chemosphere, 69 (2007) 689–696.
[12] D.W. Wang, P. Zhao, J. Yang, G.F. Xu, H.Y. Yang, Z.J. Shi, Q. Hu, Photocatalytic degradation of organic dye and phytohormone by a Cu(II) complex powder catalyst with added H_2O_2, Colloids Surf., A, 603 (2020) 125147, doi: 10.1016/j.colsurfa.2020.125147.
[13] G.M. Sheldrick, Crystal structure refinement with SHELXL, Acta Cryst., C71 (2015) 3–8.
[14] D. Zou, W.X. Feng, G.X. Shi, X.Q. Lü, Z Zhang, Y. Zhang, H. Liu, D. Fan, W.K. Wong, R.A. Jones, Hetero-binuclear near-infrared (NIR) luminescent Zn–Nd complexes self-assembled from the benzimidazole-based ligands, Spectrochim. Acta, Part A, 98 (2012) 359–366.
[15] M. Azam, S.I. Al-Resayes, S.M. Wabaidur, A. Trzesowska-Kruszynska, R. Kruszynski, R.K. Mohapatra, M.R.H. Siddiqui, Cd(II) complex constructed from dipyridyl imine ligand: design, synthesis and exploration of its photocatalytic degradation properties, Inorg. Chim. Acta, 471 (2018) 698–704.
[16] D.W. Wang, T. Wang, P. Zhao, Z.J. Shi, Q.H. Zhao, Physical characterizations, Hirshfeld surface analysis and luminescent properties of Cd(II) and Pb(II) coordination polymers based on 3-(1,2,4-triazol-1-yl)-benzoic acid, Inorg. Chim. Acta, 508 (2020) 119657, doi: 10.1016/j.ica.2020.119657.
[17] J. Liu, L. Han, H. Ma, H. Tian, J. Yang, Q. Zhang, B.J. Seligmann, S. Wang, J. Liu, Template-free synthesis of carbon doped TiO_2 mesoporous microplates for enhanced visible light photodegradation, Sci. Bull., 61 (2016) 1543–1550.
[18] S. Meghdadi, M. Amirnasr, M. Majedi, M. Bagheri, A. Amiri, S. Abbasi, K. Mereiter, Template synthesis, and X-ray crystal structures of copper(II) and nickel(II) complexes of new unsymmetrical tetradentate Schiff base ligands. Electrochemistry, antibacterial properties, and metal ion effect on hydrolysis–recondensation of the ligand, Inorg. Chim. Acta, 437 (2015) 64–69.
[19] R. Rajendran, S. Vignesh, S. Suganthi, V. Raj, G. Kavitha, B. Palanivel, M. Shkir, H. Algarni, g-C_3N_4/TiO_2/CuO S-scheme heterostructure photocatalysts for enhancing organic pollutant degradation, J. Phys. Chem. Solids, 161 (2022) 110391, doi: 10.1016/j.jpcs.2021.110391.
[20] N. Raman, A. Sakthivel, N. Pravin, Exploring DNA binding and nucleolytic activity of new 4-aminoantipyrine based amino acid Schiff base complexes: a comparative approach, Spectrochim. Acta, Part A, 125 (2014) 404–413.
[21] P. Gautam, O. Prakash, R.K. Dani, Spectra-structure correlation based study of complex molecules of 1-isonicotinoyl-3-thiosemicarbazide with Ni^{2+}, Mn^{2+} and Fe^{3+} using Raman, UV-Visible and DFT techniques, J. Mol. Struct., 1127 (2017) 489–497.
[22] Y.S. Luo, J.L. Chen, X.H. Zeng, L. Qiu, L.H. He, S.J. Liu, H.R. Wen, A highly stable and luminescent mononuclear Cu(I) bis-{5-tert-butyl-3-(6-methyl-2-pyridyl)-1H-1,2,4-triazole} complex, Chin. Chem. Lett., 28 (2017) 1027–1030.
[23] N. Aiswarya, M. Sithambaresan, S.S. Sreejith, S.W. Ng, M.R.P. Kurup, Polymeric polymorphs and a monomer of pseudohalide incorporated Cu(II) complexes of 2,4-dichlorido-6-((2-(dimethylamino)ethylimino)methyl)phenol]: crystal structures and spectroscopic behavior, Inorg. Chim. Acta, 443 (2016) 251–266.
[24] Y. Gao, J.F. Wu, J.Q. Wang, Y.X. Fan, S.Y Zhang, W. Dai, A novel multifunctional p-type semiconductor@MOFs nanoporous platform for simultaneous sensing and photodegradation of tetracycline, ACS Appl. Mater. Interfaces, 12 (2020) 11036–11044.
[25] W. Baran, E. Adamek, A. Sobczak, A. Makowski, Photocatalytic degradation of sulfa drugs with TiO_2, Fe salts and TiO_2/$FeCl_3$ in aquatic environment-kinetics and degradation pathway, Appl. Catal., B, 90 (2009) 516–525.
[26] H. Yang, G.Y. Li, T.C. An, Y.P. Gao, J.M. Fu, Photocatalytic degradation kinetics and mechanism of environmental pharmaceuticals in aqueous suspension of TiO_2: a case of sulfa drugs, Catal. Today, 153 (2010) 200–207.
[27] W.M. Zhou, S.C. Sun, Y.F. Jiang, M.X. Zhang, I. Lawan, G.F. Fernando, L.W. Wang, Z.H. Yuan, Template in situ synthesis of flower-like BiOBr/microcrystalline cellulose composites with highly visible light photocatalytic activity, Cellulose, 26 (2019) 9529–9541.
[28] H. Wang, J. Zhang, X. Yuan, L. Jiang, Q. Xia, H. Chen, Photocatalytic removal of antibiotics from natural water matrices and swine wastewater via Cu(I) coordinately polymeric carbon nitride framework, Chem. Eng. J., 392 (2020) 123638, doi: 10.1016/j.cej.2019.123638.

Supporting information

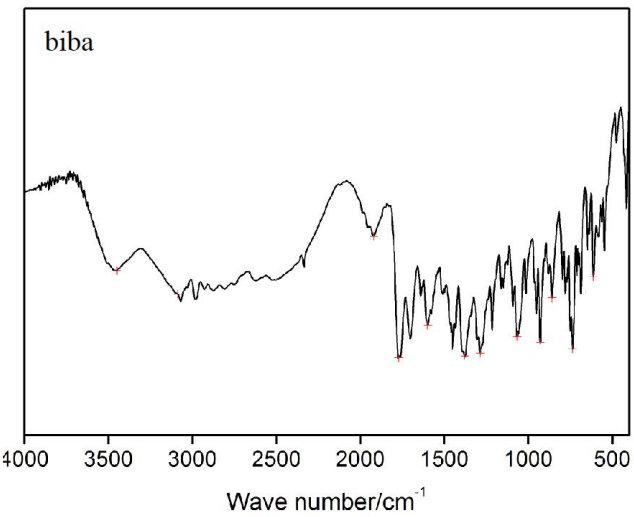

Fig. S1. IR spectrum of ligand biba.

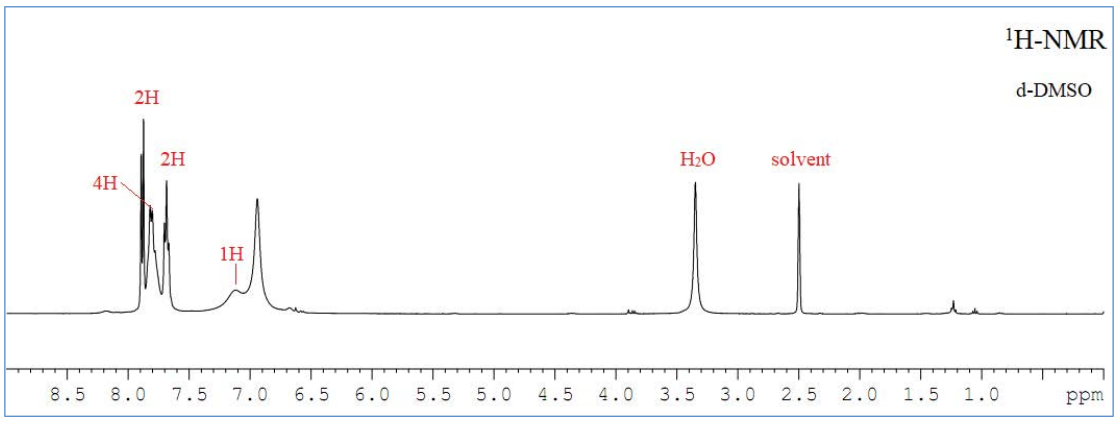

Fig. S2. ^{1}H-NMR spectrum of ligand biba (using d-DMSO as solvent).